

Final results of the Aurora experiment to study 2β decay of ^{116}Cd with enriched $^{116}\text{CdWO}_4$ crystal scintillators

A. S. Barabash,¹ P. Belli,^{2,3} R. Bernabei,^{2,3,*} F. Cappella,⁴ V. Caracciolo,⁵ R. Cerulli,^{2,3} D. M. Chernyak,^{6,7} F. A. Danevich,⁶ S. d'Angelo,^{2,3,†} A. Incicchitti,^{4,8} D. V. Kasperovych,⁶ V. V. Kobychyev,⁶ S. I. Kononov,¹ M. Laubenstein,⁵ D. V. Poda,^{6,9} O. G. Polischuk,⁶ V. N. Shlegel,¹⁰ V. I. Tretyak,⁶ V. I. Umatov,¹ and Ya. V. Vasiliev¹⁰

¹National Research Centre “Kurchatov Institute,” Institute of Theoretical and Experimental Physics, 117218 Moscow, Russia

²INFN, sezione di Roma “Tor Vergata”, I-00133 Rome, Italy

³Dipartimento di Fisica, Università di Roma “Tor Vergata”, I-00133 Rome, Italy

⁴INFN, sezione di Roma, I-00185 Rome, Italy

⁵INFN, Laboratori Nazionali del Gran Sasso, I-67100 Assergi (AQ), Italy

⁶Institute for Nuclear Research, 03028 Kyiv, Ukraine

⁷Kavli Institute for the Physics and Mathematics of the Universe, University of Tokyo, Kashiwa, 277-8583, Japan

⁸Dipartimento di Fisica, Università di Roma “La Sapienza”, I-00185 Rome, Italy

⁹CNRS/IN2P3, Université Paris-Saclay, 91405 Orsay, France

¹⁰Nikolaev Institute of Inorganic Chemistry, 630090 Novosibirsk, Russia



(Received 23 July 2018; published 12 November 2018)

The double-beta decay of ^{116}Cd has been investigated with the help of radiopure enriched $^{116}\text{CdWO}_4$ crystal scintillators (mass of 1.162 kg) at the Gran Sasso underground laboratory. The half-life of ^{116}Cd relative to the $2\nu 2\beta$ decay to the ground state of ^{116}Sn was measured with the highest up-to-date accuracy as $T_{1/2} = (2.63^{+0.11}_{-0.12}) \times 10^{19}$ yr. A new improved limit on the $0\nu 2\beta$ decay of ^{116}Cd to the ground state of ^{116}Sn was set as $T_{1/2} \geq 2.2 \times 10^{23}$ yr at 90% C.L., which is the most stringent known restriction for this isotope. It corresponds to the effective Majorana neutrino mass limit in the range $\langle m_\nu \rangle \leq (1.0\text{--}1.7)$ eV, depending on the nuclear matrix elements used in the estimations. New improved half-life limits for the $0\nu 2\beta$ decay with majoron(s) emission, Lorentz-violating $2\nu 2\beta$ decay, and 2β transitions to excited states of ^{116}Sn were set at the level of $T_{1/2} \geq 10^{20}\text{--}10^{22}$ yr. New limits for the hypothetical lepton-number violating parameters (right-handed currents admixtures in weak interaction, the effective majoron-neutrino coupling constants, R-parity violating parameter, Lorentz-violating parameter, heavy neutrino mass) were set.

DOI: [10.1103/PhysRevD.98.092007](https://doi.org/10.1103/PhysRevD.98.092007)

I. INTRODUCTION

The double-beta (2β) decay is a transformation of nucleus (A, Z) into ($A, Z + 2$) with simultaneous emission of two electrons. Two-neutrino double-beta ($2\nu 2\beta$) decay, the process allowed in the standard model of particle physics (SM), is the rarest nuclear decay ever observed (with the half-lives in the range $T_{1/2} \simeq 10^{18}\text{--}10^{24}$ yr [1–3]). Neutrinoless double-beta ($0\nu 2\beta$) decay is forbidden in the SM because it violates the lepton number by two units and is possible if neutrino is a massive Majorana particle. Therefore, the investigation of the decay is capable of clarifying many questions about neutrino and weak interaction physics: to check the lepton number

conservation, to determine the neutrino nature (Dirac or Majorana particle), to estimate an absolute scale of the neutrino mass and the neutrino mass hierarchy, to probe the existence of the right-handed currents in the weak interaction and the existence of the majorons, and to test many extensions of the SM [4–7]. After 70 years of searches, the $0\nu 2\beta$ decay remains unobserved; the most sensitive experiments give limits only on the $0\nu 2\beta$ decay half-lives for several nuclei at the level of $\lim T_{1/2} \sim 10^{24}\text{--}10^{26}$ yr. Limits on the effective Majorana neutrino mass of the electron neutrino on the level of $\lim \langle m_\nu \rangle \sim 0.1\text{--}0.7$ eV can be obtained by using theoretical calculations of the decay probability (see reviews [4,6–10] and recent results [11–17]).

Experimental investigations of the $2\nu 2\beta$ decay may test the theoretical calculations of the nuclear matrix elements (NMEs) for the $0\nu 2\beta$ decay processes [18]. In particular,

*Corresponding author.
rita.bernabei@roma2.infn.it

†Deceased.

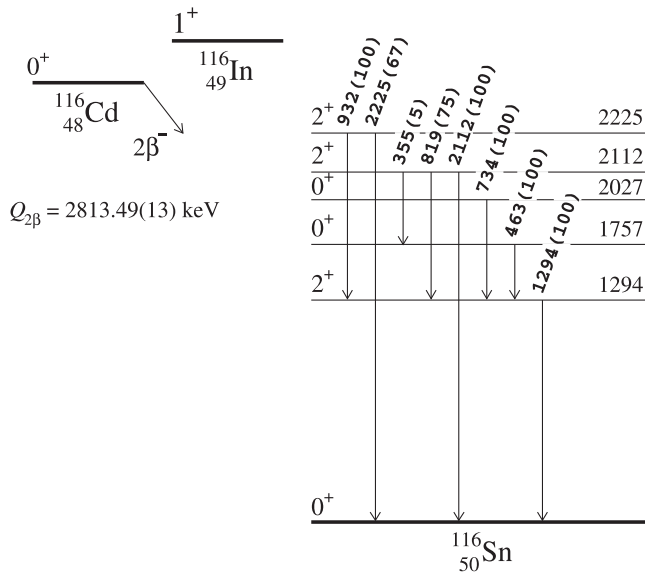


FIG. 1. Simplified decay scheme of ^{116}Cd [39]. Energies of the excited levels and emitted γ quanta are in keV. The relative intensities of γ quanta are given in parentheses.

precise measurements of the $2\nu 2\beta$ decay rate for different nuclei can help to solve problem of the axial vector coupling constant g_A value (see discussions in [4,19,20]), while accurate investigation of the $2\nu 2\beta$ decay spectral shape can help to determine the mechanism of decay (high state dominance or single state dominance [21]), to test existence of hypothetical bosonic neutrinos [22], and to check Lorentz and CPT violation [23].

The nuclide ^{116}Cd is one of the most favorable candidates for the $0\nu 2\beta$ searches thanks to the high energy of decay ($Q_{2\beta} = 2813.49(13)$ keV [24]), the promising estimations of the decay probability [19,25–29], a relatively large isotopic abundance ($\delta = 7.512(54)\%$ [30]), the availability of enrichment by ultracentrifugation in large amounts, and the possibilities to realize a calorimetric “source = detector” experiment with cadmium tungstate (CdWO_4) crystal scintillators already successfully used in several low counting

experiments [31–36]. ^{116}Cd is considered one of the most promising nuclei for a large scale bolometric experiment CUPID to explore the inverted hierarchy of the neutrino mass pattern [37,38]. A simplified scheme of ^{116}Cd 2β decay is shown in Fig. 1.

The process of two-neutrino 2β decay of ^{116}Cd was observed for the first time in the ELEGANT V experiment [40] at the Kamioka underground laboratory with the half-life $2.6_{-0.5}^{+0.9} \times 10^{19}$ yr by using drift chambers and plastic scintillators to measure electrons emitted in the decay (see Table I where the positive results of $2\nu 2\beta$ studies are presented). Then the decay was observed in the calorimetric experiment at the Solotvina underground laboratory with cadmium tungstate crystal scintillators enriched in the isotope ^{116}Cd [32,41,42]. The decay was also detected by the NEMO-2 and NEMO-3 tracking setups [43–45]. The last experiment gives up-to-date the most accurate value of the half-life $T_{1/2} = 2.74 \pm 0.04(\text{stat}) \pm 0.18(\text{sys}) \times 10^{19}$ yr [45].

The most stringent limit on $0\nu 2\beta$ decay of ^{116}Cd ($T_{1/2} \geq 1.7 \times 10^{23}$ yr at 90% confidence level, C.L.) was set in the Solotvina experiment [32]. A similar half-life limit was obtained recently by the NEMO-3 collaboration as $T_{1/2} \geq 1.0 \times 10^{23}$ yr at 90% C.L. [45]. The most sensitive searches for 2β transitions to excited levels of ^{116}Sn , and for $0\nu 2\beta$ decay with majorons emission have been also realized in the Solotvina experiment with the half-life limits on the level of $T_{1/2} \geq 10^{20}–10^{22}$ yr. The $0\nu 2\beta$ decay with majoron emission was investigated by the NEMO-3 collaboration too [45]. The 2β transitions to excited levels were also searched for by low-background γ spectrometry with high-purity germanium detectors [47,48].

Here we report the final results of the Aurora experiment to study different modes and channels of 2β decay of ^{116}Cd performed in 2011–2017 at the Gran Sasso underground laboratory with the help of more than 1 kg radiopure $^{116}\text{CdWO}_4$ crystal scintillators enriched in the isotope

TABLE I. Experiments where $2\nu 2\beta$ decay of ^{116}Cd was observed.

Experiment	$T_{1/2}(\times 10^{19}$ yr)	Year, Reference
ELEGANT V, ^{116}Cd foil, drift chambers, plastic scintillators	$2.6_{-0.5}^{+0.9}$	1995 [40]
Solotvina, $^{116}\text{CdWO}_4$ scintillators	$2.7_{-0.4}^{+0.5}(\text{stat})_{-0.6}^{+0.9}(\text{sys})$	1995 [41]
NEMO-2, ^{116}Cd foils, track reconstruction by Geiger cells, plastic scintillators	$3.75 \pm 0.35(\text{stat}) \pm 0.21(\text{sys})^a$	1995 [43,44]
Solotvina, $^{116}\text{CdWO}_4$ scintillators	$2.6 \pm 0.1(\text{stat})_{-0.4}^{+0.7}(\text{sys})$	2000 [42]
Solotvina, $^{116}\text{CdWO}_4$ scintillators	$2.9 \pm 0.06(\text{stat})_{-0.3}^{+0.4}(\text{sys})$	2003 [32]
NEMO-3, ^{116}Cd foils, track reconstruction by Geiger cells, plastic scintillators	$2.74 \pm 0.04(\text{stat}) \pm 0.18(\text{sys})$	2017 [45]
$^{116}\text{CdWO}_4$ scintillators	$2.63 \pm 0.01(\text{stat})_{-0.12}^{+0.11}(\text{sys})$	2018, Present work

^aThe result of NEMO-2 was re-estimated as $T_{1/2} = [2.9 \pm 0.3(\text{stat}) \pm 0.2(\text{sys})] \times 10^{19}$ yr in [46].

^{116}Cd . Preliminary results of the experiment were reported in the conference proceedings [49–53].

II. EXPERIMENT

Two cadmium tungstate crystals (580 g and 582 g, denoted here as No. 1 and No. 2, respectively) produced with the help of the low-thermal-gradient Czochralski crystal growth technique from highly purified cadmium enriched in ^{116}Cd to 82% [54] were used for the investigations of 2β decay of ^{116}Cd . The experiments have been realized in the low background DAMA/R&D setup installed deep underground (≈ 3600 m w.e.) at the Gran Sasso laboratory of I.N.F.N. (Italy). There were several upgrades of the experimental setup aiming at improvement of the detector background counting rate and energy resolution, and several studies about the crystal scintillators radioactive contamination [50,54–56]. In the final stage of the experiment (since 18 March 2014), the scintillators were fixed inside polytetrafluoroethylene containers (see a schematic cross-sectional view of the Aurora setup in Fig. 2) filled up with ultra-pure pseudocumene based liquid scintillator (LS). The $^{116}\text{CdWO}_4$ crystals and the LS were viewed through high-purity quartz light guides ($\varnothing 7 \times 40$ cm) by 3 inches low radioactive photomultiplier tubes (PMT, Hamamatsu R6233MOD). The detector was installed inside a passive shield assembled from high-purity copper (10 cm), low radioactive lead (15 cm), cadmium (1.5 mm) and polyethylene/paraffin (4 to 10 cm) to reduce the external background. The

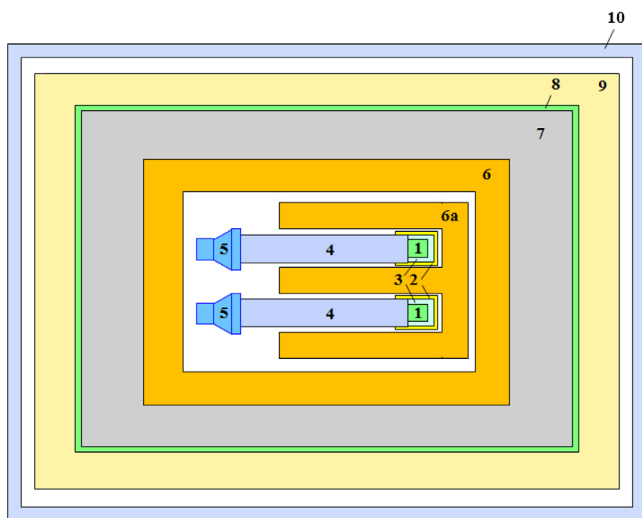


FIG. 2. Schematic cross-sectional view of the Aurora setup. There were $^{116}\text{CdWO}_4$ crystal scintillators (1) fixed in Teflon containers (2) filled up with liquid scintillator (3) and viewed through quartz light guides (4) by photomultipliers (5). The passive shield consisted of high-purity copper (6), an additional high-purity copper shield (6a), low radioactive lead (7), cadmium (8), polyethylene/paraffin (9), and a plexiglas box (10).

whole setup was contained inside a plexiglas box and continuously flushed by high-purity nitrogen gas to remove environmental radon.

An event-by-event data acquisition system (DAQ) based on a 1 GS/s 8-bit transient digitizer (Acqiris DC270) recorded the amplitude, the arrival time and the pulse shape of each event (over $50 \mu\text{s}$ with a time bin of 20 ns). Multiple events were acquired in a single buffer in the DAQ program (190 events per each buffer, without dead time). The energy scale and the energy resolution of the detectors were measured in the beginning, several times during the measurements, and at the end of the experiment with ^{22}Na , ^{60}Co , ^{133}Ba , ^{137}Cs , and ^{228}Th γ sources. The data of the calibration measurements were used to set a dependence of the energy resolution on energy. The energy resolution of the detector to γ quanta with energy E_γ can be described by the function $\text{FWHM}_\gamma = \sqrt{10.2 \times E_\gamma}$, where FWHM_γ (Full Width at Half Maximum) and E_γ are given in keV. The energy scale during the experiment was reasonably stable with deviation in the range of $\pm 0.9\%$.

III. DATA ANALYSIS

The pulse-shape discrimination (PSD) between $\gamma(\beta)$ and α particles, the time-amplitude analysis of fast subchains of decays from the ^{232}Th family, the front-edge analysis of the pulse shape, and the Monte Carlo simulation of the measured energy spectra have been applied to estimate the radioactive contamination of the $^{116}\text{CdWO}_4$ crystal scintillators, the response of the detector to α particles, and to reject the detectors background. The data on radioactive contamination of the $^{116}\text{CdWO}_4$ crystal scintillators were then used to build a model of the background that is a crucial issue to estimate the ^{116}Cd half-life relative to the two-neutrino mode of 2β decay and derive limits on the 2β processes that have not been observed.

A. Pulse-shape discrimination between $\gamma(\beta)$ and α particles

The optimal filter method proposed by E. Gatti and F. De Martini [57], developed for CdWO_4 scintillation detectors [58,59], was applied to analyze the pulse profiles of the events aiming at discrimination of $\gamma(\beta)$ events from those induced by α particles. For each signal $f(t)$, the numerical characteristic of its shape (shape indicator, SI) was defined by using the following equation:

$$SI = \sum f(t_k) \times P(t_k) / \sum f(t_k), \quad (1)$$

where the sum is over the time channels k , starting from the origin of signal up to $50 \mu\text{s}$; $f(t_k)$ is the digitized amplitude (at the time t_k) of a given signal. The weight function $P(t)$ was defined as:

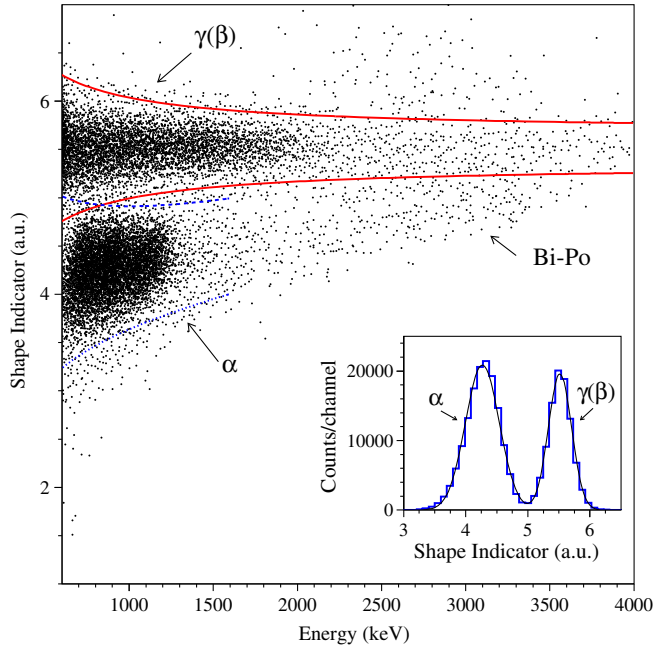


FIG. 3. Shape indicator (see text) versus energy for the background data accumulated over 26831 h with the $^{116}\text{CdWO}_4$ crystal scintillator No. 2. The 2.33-sigma intervals (98% of events) for the shape indicator values corresponding to $\gamma(\beta)$ and α particles are depicted by solid and dotted lines, respectively. The population of events in the energy interval $\sim(1.7\text{--}4)$ MeV with shape indicator values between $\sim(4\text{--}7)$ are caused by the decays of the fast $^{212}\text{Bi}\text{--}^{212}\text{Po}$ subchain of the ^{232}Th chain. (inset) Distribution of shape indicators for the events with the energies in the range of 0.7–1.4 MeV. The fit of the distribution by Gaussian functions is shown by solid line.

$$P(t) = |f_\alpha(t) - f_\gamma(t)| / |f_\alpha(t) + f_\gamma(t)|, \quad (2)$$

where $f_\alpha(t)$ and $f_\gamma(t)$ are the reference pulse shapes for α particles and γ quanta, respectively. By using this approach, α events were clearly separated from $\gamma(\beta)$ events. The scatter plot of the shape indicator versus energy for the data of the low background measurements is shown in Fig. 3; it demonstrates the pulse-shape discrimination ability of the $^{116}\text{CdWO}_4$ detector. The distribution of shape indicators for the events with the energies in the range of 0.7–1.4 MeV is shown in inset of Fig. 3. The spectra of $\gamma(\beta)$ and α events selected by the pulse-shape analysis are presented in Fig. 4. The total alpha activity of U/Th with their daughters in the crystal No. 2 is higher than that in the crystal No. 1 due to segregation of impurities (particularly of radioactive elements) in the crystal growth process [60]. The total internal α activity in the crystals No. 1 and No. 2 is 1.8(2) mBq/kg and 2.7(3) mBq/kg, respectively.

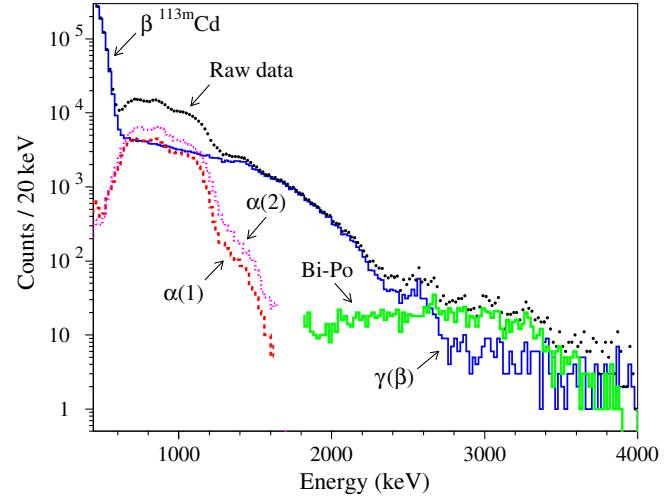


FIG. 4. The sum energy spectrum acquired with two $^{116}\text{CdWO}_4$ detectors over 26831 h (Raw data) and spectra of $\gamma(\beta)$, α and $^{212}\text{Bi}\text{--}^{212}\text{Po}$ events (denoted “Bi-Po”) selected by the pulse-shape and the front-edge analyzes described in text (for the front-edge analysis, see Sec. III C). The spectra $\alpha(1)$ and $\alpha(2)$ denote the distributions of alpha events accumulated by the detectors No. 1 and No. 2, respectively.

A sum α energy spectrum of the two detectors (see Fig. 5) was fitted by using a model which includes α peaks of ^{232}Th , ^{238}U and their daughters, plus γ/β background. The equilibrium of the ^{232}Th and ^{238}U chains is assumed to be broken in the $^{116}\text{CdWO}_4$ crystals. Therefore, activities of ^{238}U , ^{234}U , ^{230}Th , ^{226}Ra , ^{210}Po , ^{232}Th , ^{228}Th were free parameters of the fit. We have found that the spectral shape

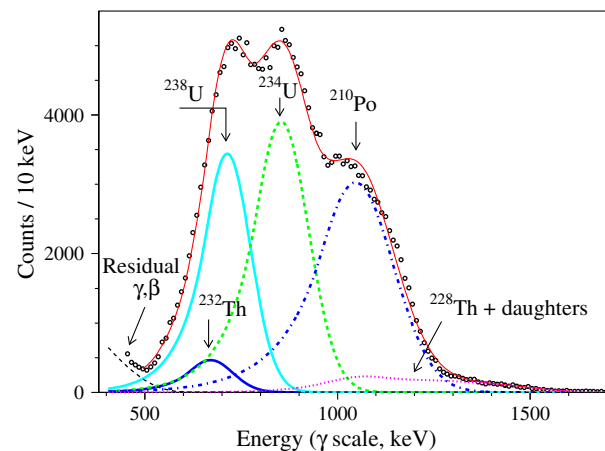


FIG. 5. The sum energy spectrum of α events (points) selected by the pulse-shape discrimination from the data of low-background measurements with the $^{116}\text{CdWO}_4$ crystal scintillators No. 1 and No. 2 over 26831 h. The fit of the data by the model built from α decays of ^{238}U and ^{232}Th with daughters, and residual γ , β background is shown by solid line (the individual components of the fit are shown too).

TABLE II. Radioactive contamination of the $^{116}\text{CdWO}_4$ crystals. Reference date is February 2016.

Chain	Nuclide	Activity (mBq/kg)
	^{40}K	0.22(9)
	$^{90}\text{Sr} - ^{90}\text{Y}$	≤ 0.02
	^{110m}Ag	≤ 0.007
	^{116}Cd	1.138(5)
^{232}Th	^{232}Th	0.07(2)
	^{228}Ra	≤ 0.005
	^{228}Th	0.020(1)
^{235}U	^{227}Ac	≤ 0.002
^{238}U	^{238}U	0.58(4)
	^{234}U	0.6(1)
	^{230}Th	≤ 0.13
	^{226}Ra	≤ 0.006
	^{210}Pb	0.70(4)
Total α		2.14(2)

of the individual alpha peaks is described better by using the asymmetrical function proposed in [61] (see Sec. IIIB). The energy resolution of the detector to α particles and the α/γ ratio¹ were taken as free parameters of the fit. Furthermore, we should use different α/γ ratio and energy resolution to describe peak of ^{210}Po in the spectrum, that can be explained by nonuniform distribution of different impurities in the crystals volume, particularly of ^{210}Pb that is parent nuclide for ^{210}Po . The effect can be explained by two possible origins of ^{210}Pb in the crystals: as lead impurity (since lead always contains some amount of radioactive ^{210}Pb), and as product of radium decay (isotope ^{226}Ra , daughter of ^{238}U). Besides, one cannot exclude surface contamination of the crystals by ^{210}Pb caused by decays of radon present in air. Both α/γ ratio and energy resolution are higher for the ^{210}Po α peak than that for other α active nuclides.

The result of the fit in the energy interval (470–1600) keV is shown in Fig. 5. The fit gives the activities of ^{238}U , ^{234}U , ^{210}Po , ^{232}Th and ^{228}Th in the crystals presented in Table II, while only limits were obtained for the activity of ^{230}Th and ^{226}Ra (the activity of ^{228}Th was then estimated with a higher accuracy with the help of the time-amplitude and front-edge analyzes, Secs. IIIB and IIIC). The reference date (February 2016) is given to take into account the decay of ^{228}Th (the half-life is $T_{1/2} = 1.9116$ yr) and ^{110m}Ag ($T_{1/2} = 249.83$ d) in the crystals.

¹The α/γ ratio is the light yield of α particles LY_α divided by light yield of gamma quanta LY_γ of the same energy. Because of quenching, LY for heavy particles in scintillators is lower than that for electrons (or γ quanta), depending on the particle's type and energy [62].

B. TIME-AMPLITUDE ANALYSIS OF FAST SUBCHAINS

1. Selection of the $^{224}\text{Ra} \rightarrow ^{220}\text{Rn} \rightarrow ^{216}\text{Po} \rightarrow ^{212}\text{Pb}$ Pb subchain

The time-amplitude analysis (described e.g., in [31,63,64]) was used to select events of the following decay subchain of the ^{232}Th family:

$$^{224}\text{Ra}(Q_\alpha = 5789 \text{ keV}; T_{1/2} = 3.632 \text{ d}) \\ \rightarrow ^{220}\text{Rn}(Q_\alpha = 6405 \text{ keV}; T_{1/2} = 55.6 \text{ s}) \rightarrow ^{216}\text{Po} \\ (Q_\alpha = 6906 \text{ keV}; T_{1/2} = 0.145 \text{ s}) \rightarrow ^{212}\text{Pb}.$$

To select decays of the subchain, all α events within an energy interval 0.82–1.54 MeV were used as triggers (α particles of ^{220}Rn), while a time interval 0–0.725 s and the 0.96–1.72 MeV energy window were set for the second α events (^{216}Po). Taking into account the efficiency of the events selection in this time interval (96.88% of ^{216}Po decays), the activity of ^{228}Th in the $^{116}\text{CdWO}_4$ crystals No. 1 and No. 2 was calculated as 0.013(3) mBq/kg and 0.029(4) mBq/kg, respectively. All the selected pairs $^{220}\text{Rn} - ^{216}\text{Po}$ were used as triggers to find events of ^{224}Ra α decay. A 0–111 s time interval was chosen to select events in the energy interval 0.66–1.36 MeV. The obtained α peaks from the $^{224}\text{Ra} \rightarrow ^{220}\text{Rn} \rightarrow ^{216}\text{Po} \rightarrow ^{212}\text{Pb}$

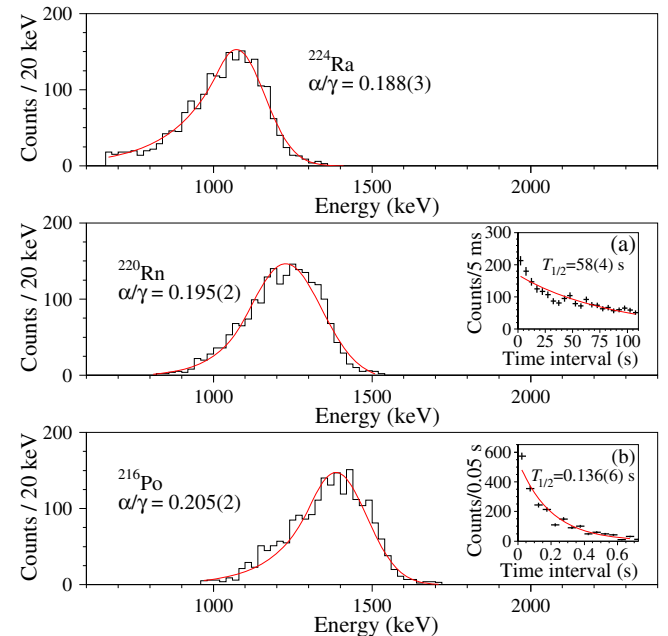
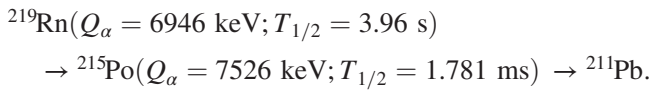


FIG. 6. Alpha peaks of ^{224}Ra , ^{220}Rn and ^{216}Po selected by the time-amplitude analysis from the data accumulated over 26831 h with the $^{116}\text{CdWO}_4$ detectors No. 1 and No. 2. The obtained half-lives of ^{220}Rn , 58 ± 4 s, inset (a), and ^{216}Po , 0.136 ± 0.006 s, inset (b), are in agreement with the table values (55.6 ± 0.1 s and 0.145 ± 0.002 s, respectively).

subchain and the time distributions for the $^{220}\text{Rn} \rightarrow ^{216}\text{Po}$ and $^{216}\text{Po} \rightarrow ^{212}\text{Pb}$ decays in the $^{116}\text{CdWO}_4$ detectors No. 1 and No. 2 are shown in Fig. 6. The estimated half-lives of ^{220}Rn and ^{216}Po are in agreement with those table values. An averaged activity of ^{228}Th in the $^{116}\text{CdWO}_4$ crystal scintillators estimated by using the time-amplitude analysis is given in Table II. It should be stressed that the fit of the alpha spectra were performed using non-Gaussian function for individual α peaks proposed in [61]. The non-Gaussian shape of the peaks can be explained by the nonuniformity of the U/Th impurities concentration in the crystals [60] and, as a result, by nonuniformity of the light collection in the detector's volume.

No events were found with the time-amplitude analysis aiming at search for the following fast subchain of the ^{235}U family (expected to be in equilibrium with ^{227}Ac):



As a result we set a limit on activity of ^{227}Ac in the crystals on the level of $\leq 0.002 \text{ mBq/kg}$.

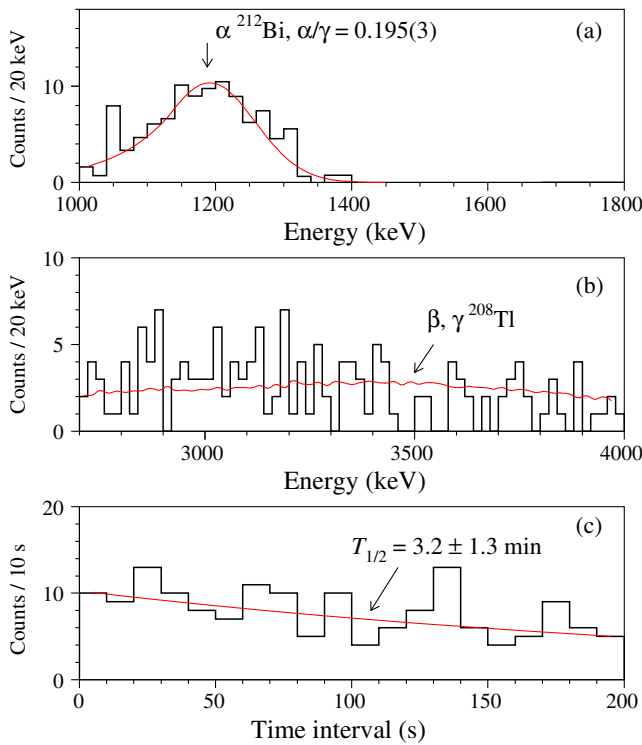


FIG. 7. The energy (a) and (b), and time (c) distributions for the sequence of α (^{212}Bi) and β, γ (^{208}Tl) decays selected from the data accumulated over 26831 h with the $^{116}\text{CdWO}_4$ detectors No. 1 and No. 2. The fit of the α peak (a), the approximation of the energy distribution by a Monte Carlo simulated distribution of ^{208}Tl events (b), and the fit of the time distribution by an exponential function with the half-life 3.2(13) minutes (c) are shown.

2. Selection of $^{212}\text{Bi} \rightarrow ^{208}\text{Tl}$ events

The following chain of decays: $^{212}\text{Bi}(Q_\alpha = 6207 \text{ keV}) \rightarrow ^{208}\text{Tl}(Q_\beta = 4999 \text{ keV}, T_{1/2} = 3.053 \text{ min}) \rightarrow ^{208}\text{Pb}$ was selected by using the time-amplitude analysis. All α events within the energy interval 1.0–1.4 MeV (which contains α peak of ^{212}Bi) were used as triggers, and all the subsequent γ/β events in the energy interval 2.7–4.0 MeV were selected within a time interval (0.0001–200) s (containing 53% of ^{208}Tl decays). The capability of the analysis is demonstrated in Fig. 7. The alpha peak of ^{212}Bi was fitted by the asymmetric function [61] giving the α/γ ratio 0.195(3). The distribution of the second events is well described by the simulated spectrum of β and γ events of ^{208}Tl , while the distribution of time intervals between the events can be approximated by exponential function with the half-life $3.2 \pm 1.3 \text{ min}$, in a reasonable agreement with the table value for ^{208}Tl .

The selection procedure reduces the background in the high-energy part of the spectrum of β and γ events, however, the procedure decreases also the live time of measurements. For this reason, the data obtained after subtraction of the ^{208}Tl events were not used for estimations of double-beta processes in ^{116}Cd .

By using positions of the α peaks of ^{224}Ra , ^{220}Rn and ^{216}Po (from the time-amplitude analysis, see Fig. 6), of ^{232}Th , ^{238}U and ^{234}U (from the pulse-shape discrimination, see Fig. 5) and of ^{212}Bi (obtained by the analysis of the sequence $^{212}\text{Bi} - ^{208}\text{Tl}$ presented in Fig. 7), the following dependence of α/γ ratio on energy of α particles was obtained: $\alpha/\gamma = 0.114(7) + 0.0133(12)E_\alpha$ in the energy interval 4.0–6.8 MeV (E_α is in MeV). The dependence of the α/γ ratio on energy of α particles is presented in Fig. 8.

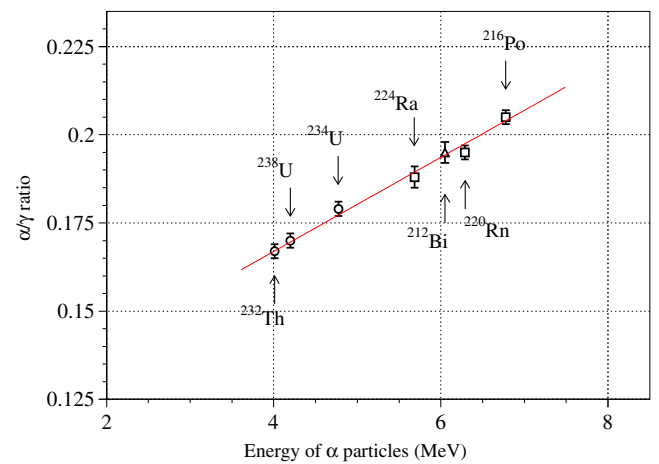


FIG. 8. Dependence of α/γ ratio on energy of the α particles. The open circles are from the PSD (Fig. 5), the open squares are from the time-amplitude analysis (Fig. 6), and the triangle is obtained by the analysis of the sequence $^{212}\text{Bi} - ^{208}\text{Tl}$ (Fig. 7).

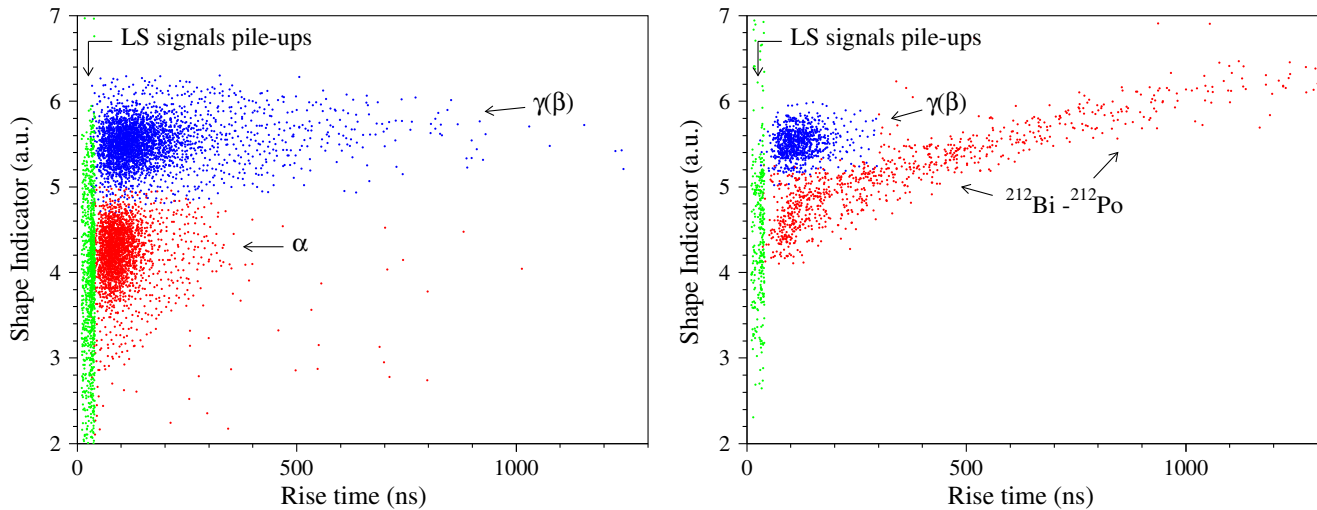
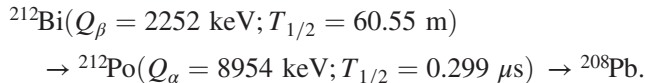


FIG. 9. Distributions of shape indicator versus rise time for the background events acquired with the $^{116}\text{CdWO}_4$ detector No. 2 over 26831 h in the energy interval 0.6–1.3 MeV (left panel) and in the energy interval 1.7–4.0 MeV (right panel).

C. Discrimination of $^{212}\text{Bi} - ^{212}\text{Po}$ events by front-edge analysis

The front-edge analysis was developed to reject the following fast subchain of decays from the ^{232}Th family (Bi-Po events):



A front-edge parameter (rise time) for each signal was calculated as time between the signal origin and the time where signal reach 0.7 of its maximal value. Results of the front-edge analysis are illustrated in Fig. 9, where the scatter plots of the shape indicator versus pulse rise time for the background data gathered over 26831 h with the $^{116}\text{CdWO}_4$ detector No. 2 are shown for the events selected in the energy intervals 0.6–1.3 MeV and 1.7–4.0 MeV. The 1.7–4.0 MeV data contain events with longer rise time that is in agreement with an expected sum energy release in the $^{212}\text{Bi} - ^{212}\text{Po}$ decay $\sim 1.8\text{--}4.4$ MeV. An energy spectrum of the $^{212}\text{Bi} - ^{212}\text{Po}$ events selected by the front-edge analysis is shown in Fig. 4. It should be stressed that $^{212}\text{Bi} - ^{212}\text{Po}$ events are also visible in Fig. 3 since the PSD analysis is sensitive to these events too.

The analysis allowed to estimate the activity of ^{212}Bi (which is in equilibrium with ^{228}Th) in the crystals No. 1 and No. 2 as 0.018(2) mBq/kg and 0.027(3) mBq/kg, respectively, in a reasonable agreement with the results of the time-amplitude analysis (Sec. III B). All the selected Bi-Po events were discarded from the data that reduced background counting rate in the energy region of interest (2.7–2.9 MeV) by a factor of ~ 1.5 .

It should be stressed that the front-edge analysis also rejects pile-ups of liquid scintillator pulses with $^{116}\text{CdWO}_4$

signals thanks to a shorter rise time (less than 38 ns; see Fig. 9) of the liquid scintillator pulses.

IV. RESULTS AND DISCUSSION

A. $2\nu 2\beta$ decay of ^{116}Cd to the ground state of ^{116}Sn

The energy spectrum of $\gamma(\beta)$ events selected by using the PSD and front-edge analyzes was corrected taking into account the efficiency of the simultaneous application of the PSD and front-edge discrimination cuts presented in Fig. 10. The corrected data accumulated over 26831 h with the two $^{116}\text{CdWO}_4$ detectors are shown in Fig. 11. There is a clear signature of the ^{116}Cd $2\nu 2\beta$ decay distribution in the data.

To estimate a half-life of ^{116}Cd relative to the $2\nu 2\beta$ decay, the spectrum was fitted by the background model built from internal ^{40}K , ^{90}Sr , ^{90}Y (^{90}Y was assumed to be in equilibrium with ^{90}Sr), ^{110m}Ag ,² beta active daughters of ^{232}Th and ^{238}U , external gamma quanta from radioactive contamination of the setup by potassium, thorium and radium (radioactive contamination of the copper shield, PMTs, and the quartz light guides were taken as free parameters), and the $2\nu 2\beta$ decay of ^{116}Cd . All the models were simulated by using the EGS4 simulation package [65], the initial kinematics of the particles emitted in the decays was given by an event generator DECAY0 [66]. The energy distribution of the $2\nu 2\beta$ decay of ^{116}Cd (in total 5×10^6 decays were simulated in the both detectors) contains 98.86% of the simulated events. The loss of 1.14% events is due to rejection of escaped β particles and bremsstrahlung γ

²Despite the long time after the crystal was produced in the end of 2010, we cannot exclude presence of cosmogenic nuclides (particularly of ^{110m}Ag that was observed in the crystals in the early measurements [54]) since the scintillators were several times moved to surface for treatment and the detector upgrade.

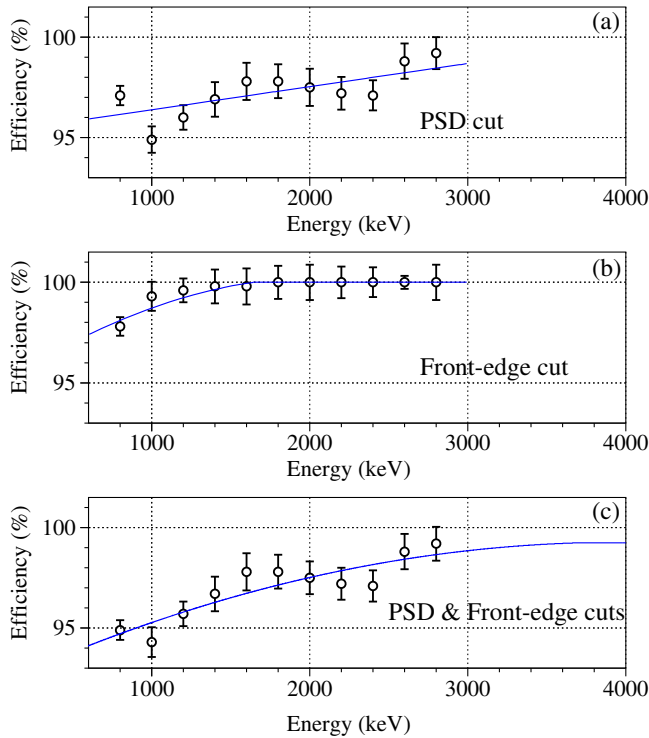


FIG. 10. Efficiencies measured for γ rays from ^{228}Th calibration source when applying the pulse-shape discrimination cut (a), the front-edge analysis cut (b) and both of them (c).

quanta by the liquid scintillator surrounding the $^{116}\text{CdWO}_4$ scintillators.

The experimental spectrum was fitted in the energy intervals within (640–1600) keV, for the starting point, and (2800–3600) keV, for the final point, with a step 20 keV that gives the $\chi^2/\text{n.d.f.}$ values (where n.d.f. is the number of degrees of freedom) within 1.15–1.75. The best fit ($\chi^2/\text{n.d.f.} = 142/124 = 1.15$) was achieved in the energy interval (720–3560) keV giving 126341 counts of the $2\nu 2\beta$ decay of ^{116}Cd in the whole spectrum with a statistical error 527 counts. The energy interval contains 73.55% of the whole $2\nu 2\beta$ distribution, the effect to background ratio is approximately 1.5. Using the number of $2\nu 2\beta$ events, activity of ^{116}Cd in the $^{116}\text{CdWO}_4$ crystals is 1.138(5) mBq/kg (only statistical error). The activity is presented in Table II together with activity of ^{40}K , and limits on activities of ^{110m}Ag , $^{90}\text{Sr} - ^{90}\text{Y}$, ^{228}Ra and ^{226}Ra obtained from the fits. Taking into account the number of ^{116}Cd nuclei in the crystal scintillators ($N = 1.584 \times 10^{24}$), the half-life of ^{116}Cd relative to the $2\nu 2\beta$ decay to the ground state of ^{116}Sn is (only statistical error):

$$T_{1/2} = (2.630 \pm 0.011) \times 10^{19} \text{ yr.}$$

The main contribution to the systematic error comes from the ambiguity of the background model, first of all, from the uncertainty of radioactive contamination of the

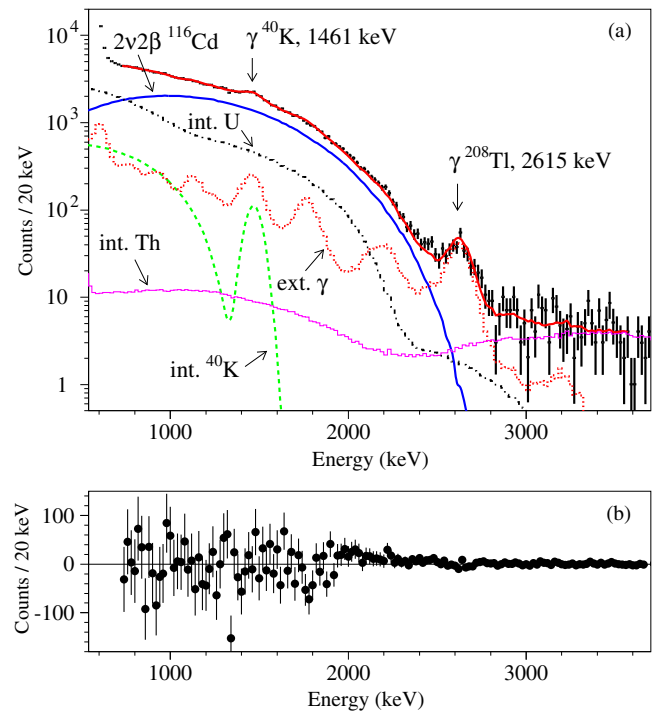


FIG. 11. The energy spectrum of $\gamma(\beta)$ events accumulated over 26831 h with the $^{116}\text{CdWO}_4$ detectors together with the main components of the background model: the $2\nu 2\beta$ decay of ^{116}Cd (“ $2\nu 2\beta$ ”), internal contaminations of the $^{116}\text{CdWO}_4$ crystals by U/Th, K (“int. U”, “int. Th”, “int. ^{40}K ”), and contributions from external γ quanta (“ext. γ ”) (a). The difference between the experimental energy spectrum and the Monte Carlo background model (b).

$^{116}\text{CdWO}_4$ crystals by ^{238}U , since the β spectrum of ^{234m}Pa (daughter of ^{238}U) competes with the $2\nu 2\beta$ spectrum of ^{116}Cd (see Fig. 11 where the result of fit and the main background components are shown). The estimations of the contribution to the systematic error of uncertainties of the internal radioactive contamination of the $^{116}\text{CdWO}_4$ crystal scintillators and the external background from the details of the setup are given in Table III. We assume that errors of the internal radioactive contamination activities contribute to the systematic error of the background model. If only limit on activity is known (the case of $^{90}\text{Sr} - ^{90}\text{Y}$, ^{110m}Ag , ^{228}Ra , ^{226}Ra) the number of counts \pm error was taken in the range from zero to the limit. Despite we cannot determine exact activities of radioactive contamination in the setup details, the error of the external background model was taken from the fit, since there are gamma peaks in the energy spectrum that justify the radioactive contamination even if its exact localization remains unknown.

To take into account imprecise knowledge of the setup radioactive contaminations localization, we have fitted the energy spectrum presented in Fig. 11 by three “extreme” models with radioactive contaminations localized in different details of the setup: (1) all the potassium, thorium and

TABLE III. Contribution to the $T_{1/2}^{2\nu2\beta}$ systematic error of the background model components due to internal contamination of the $^{116}\text{CdWO}_4$ crystals and external background. The number of counts in the experimental spectrum is given too. The errors in the 3rd column are calculated in % of the ^{116}Cd half-life.

Component of the background model	Number of counts in the energy interval of fit (720–3560) keV	Contribution to $T_{1/2}^{2\nu2\beta}$ error (%)
Experimental data	154956	...
$2\nu2\beta$	92923	...
^{40}K	6623 ± 685	± 0.74
$^{90}\text{Sr} - ^{90}\text{Y}$	3_{-3}^{+1403}	+1.51
^{110m}Ag	170_{-170}^{+114}	+0.12 -0.18
^{228}Ac	117_{-117}^{+173}	+0.19 -0.13
^{228}Th ($^{212}\text{Bi} + ^{208}\text{Tl}$)	714 ± 55	± 0.06
^{234m}Pa	33129 ± 2455	± 2.64
^{226}Ra ($^{214}\text{Pb} + ^{214}\text{Bi}$)	500_{-500}^{+39}	+0.04 -0.54
^{210}Bi	9244 ± 550	± 0.59
Internal background model	50500_{-2663}^{+2969}	+3.19 -2.87
External background model	11388 ± 557	± 0.60
Model of background (total)	61888_{-2721}^{+3021}	+3.25 -2.93

radium contaminations are in the PMTs, (2) all are in the copper shield, and (3) all are in the quartz light guides. The extreme cases give estimation of the systematic error due to the ambiguity of the radioactive-contamination localization $_{-2.63}^{+1.54}$ % (see Table IV). It should be stressed that the “extreme” fits are characterized by bigger values of $\chi^2/\text{n.d.f.}$, that confirms our quite natural assumption that all the details of the setup (at least the ones, included in the background model) have their own contamination. The variation of the ^{116}Cd half-life depending on the energy interval of fit was estimated as $_{-1.02}^{+0.34}$ %. In fact, these errors are also related to the uncertainty of the background model.

The error due to the detector energy scale instability is estimated to be $\pm 1.72\%$. Then we assume that possible uncertainties in the theoretical $2\nu2\beta$ decay spectral shape contribute to the systematic error on the level of 1% [67].

Finally, uncertainties of the PSD and front-edge analyzes cuts and number of ^{116}Cd nuclei contribute to the systematic error too. All the systematic uncertainties of the $T_{1/2}$ are summarized in Table IV.

By summing all the systematic errors in square we obtain the following half-life of ^{116}Cd relative to the $2\nu2\beta$ decay to the ground state of ^{116}Sn :

$$T_{1/2} = [2.630 \pm 0.011(\text{stat})_{-0.123}^{+0.113}(\text{sys})] \times 10^{19} \text{ yr.}$$

Taking into account a comparatively small statistical error, the final half-life value can be obtained by summing the errors in quadrature:

TABLE IV. Systematic uncertainties of $T_{1/2}$ (%).

Source	Contribution
Number of ^{116}Cd nuclei	± 0.12
PSD and front-edge cuts efficiency	± 1.2
Model of background	+3.25 -2.93
Localization of radioactive contaminations	+1.54 -2.63
Interval of the fit	+0.34 -1.02
Energy scale instability	± 1.72
$2\nu2\beta$ spectral shape	± 1.0
Total systematic error	+4.30 -4.69

$$T_{1/2} = (2.63_{-0.12}^{+0.11}) \times 10^{19} \text{ yr.}$$

The obtained half-life value is compared with the results of other experiments in Table I and Fig. 12.

The higher precision of the half-life value in the Aurora experiment was achieved thanks to the certain advantages of the radiopure, enriched in the isotope ^{116}Cd scintillation detectors: a high, accurately defined detection efficiency, in contrast to the tracking experiments [40,44] where detection efficiency depends on many factors and typically cannot be estimated so precisely. In addition, the ^{116}Cd scintillation detectors used in the present study have almost a twice higher energy resolution than that in the Solotvina experiments (which also utilized enriched $^{116}\text{CdWO}_4$ crystal scintillators, however of a lower quality [32,41,42]). The higher energy resolution, particularly to α particles, together with the higher exposure of the experiment, allowed to estimate the ^{238}U activity in the $^{116}\text{CdWO}_4$

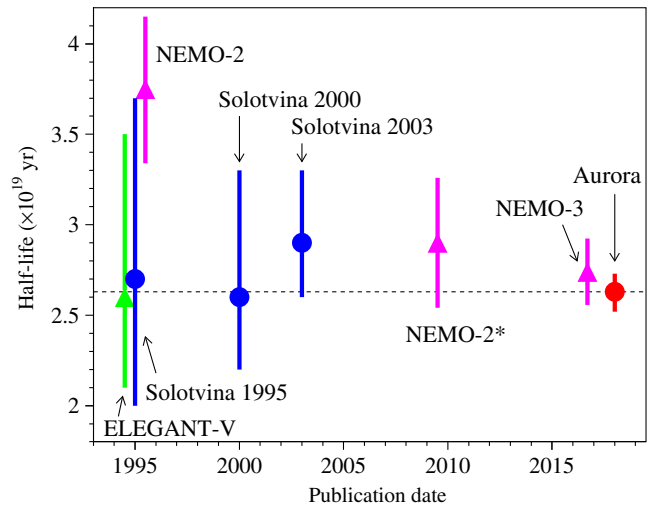


FIG. 12. Comparison of the ^{116}Cd $2\nu2\beta$ half-life obtained in the Aurora experiment with other experiments: ELEGANT V [40], Solotvina (three stages of the experiment published in 1995, 2000 and 2003) [32,41,42], NEMO-2 [44], and NEMO-3 [45]. A re-estimation of the NEMO-2 experiment (NEMO-2*) [46] is shown too.

crystal scintillators with a relative error $\approx 7\%$ (while only the total alpha activity was estimated in the $^{116}\text{CdWO}_4$ scintillators used in the Solotvina experiments). The knowledge of the activity, and therefore, activity of its daughter β active ^{234m}Pa (that competes with the $2\nu 2\beta$ spectrum of ^{116}Cd), allowed to reduce the model of background uncertainty that is the main source of systematic error in the scintillation experiments.

By using the half-life one can estimate an effective NME^{eff} for the $2\nu 2\beta$ decay of ^{116}Cd to the ground state of ^{116}Sn by using the following equation:

$$NME^{\text{eff}} = 1/\sqrt{G_{2\nu 2\beta} \times T_{1/2}}, \quad (3)$$

where $G_{2\nu 2\beta}$ is the phase space factor. Effective nuclear matrix elements calculated by using the space factor from [68,69] are presented in Table V.

B. Search for $0\nu 2\beta$ decay of ^{116}Cd

There are no peculiarities in the experimental data which could be ascribed to other possible 2β processes in ^{116}Cd . A lower limit on the half-life of ^{116}Cd relative to different 2β decay channels and modes can be estimated by using the following equation:

$$\lim T_{1/2} = N \cdot \eta \cdot t \cdot \ln 2 / \lim S, \quad (4)$$

where N is the number of ^{116}Cd nuclei in the $^{116}\text{CdWO}_4$ crystal scintillators, η is the detection efficiency for the process of decay, t is the time of measurements, and $\lim S$ is the number of events of the effect searched for, which can be excluded at a given C.L.

To estimate a limit on the half-life of ^{116}Cd relative to $0\nu 2\beta$ decay to the ground state of ^{116}Sn , we included in the analysis also the data from the previous stage of the experiment over 8493 h with a similar background counting rate of ≈ 0.1 counts/(keV kg yr) in the energy interval 2.7–2.9 MeV. Those data were not used for the analysis of the $2\nu 2\beta$ decay of ^{116}Cd due to a much higher background counting rate caused by rather high contamination of the Ultima Gold liquid scintillator (surrounding the $^{116}\text{CdWO}_4$ crystal scintillators) by potassium. The scintillator was replaced by the radiopure one in the further stages of the experiment.

TABLE V. Effective nuclear matrix elements for $2\nu 2\beta$ decay of ^{116}Cd to the ground state of ^{116}Sn obtained by using different calculations of the phase space factors.

Phase space factor (10^{-21} yr $^{-1}$), Reference	Effective nuclear matrix element
2764 [68]	$0.1173^{+0.0027}_{-0.0024}$
3176 [68] (SSD model)	$0.1094^{+0.0025}_{-0.0023}$
2688 [69]	$0.1189^{+0.0027}_{-0.0025}$

The sum energy spectrum over 35324 h with the background counting rate 0.146(12) counts/(keV yr kg), corrected for the efficiency of the PSD analysis (Fig. 10, c), is presented in Fig. 13. The spectrum was approximated in the energy intervals (2.1–2.3) MeV—(3.3–3.7) MeV with a step 20 keV by the background model constructed from the distributions of the $0\nu 2\beta$ decay (an effect searched for), $2\nu 2\beta$ decay of ^{116}Cd with the half-life $2.63^{+0.11}_{-0.12} \times 10^{19}$ yr, the internal contamination of the crystals by ^{110m}Ag , ^{228}Th and ^{234m}Pa (bounded within the values or limits presented in Table II), and the contribution from external γ quanta from contamination of the setup by radium (only ^{214}Bi was considered due to the large enough energy of β decay) and thorium (^{208}Tl). The best fit ($\chi^2/\text{n.d.f.} = 70.6/70 = 1.01$) achieved in the energy interval 2160–3740 keV gives an area of the peak searched for $S = -4.5 \pm 14.2$ counts, that is no evidence of the effect. It should be stressed that the fit of the peak area (i.e., $S = -4.5 \pm 14.2$ counts) includes only statistical errors coming from the data fluctuations, and that systematic contributions have not been included in the quoted value of the peak area error obtained with

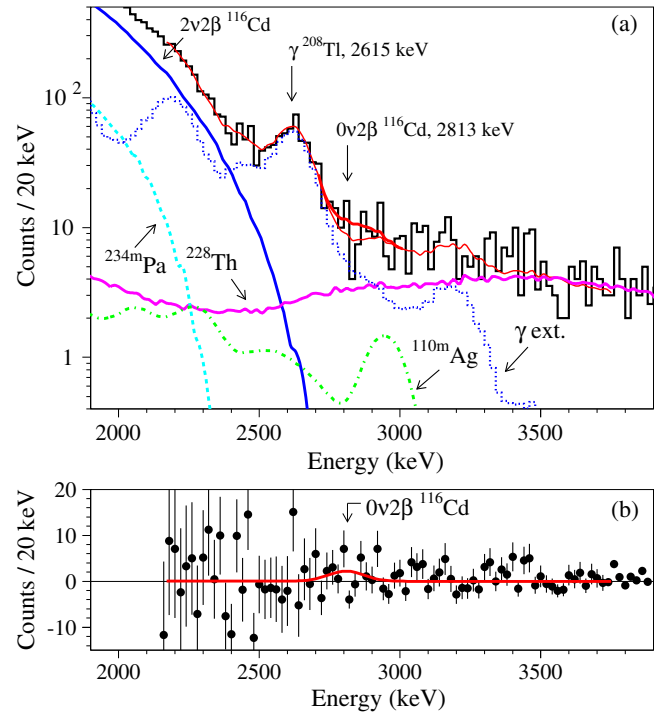


FIG. 13. Part of the energy spectrum of $\gamma(\beta)$ events accumulated over 35324 h with the $^{116}\text{CdWO}_4$ detectors together with the background model: the $2\nu 2\beta$ decay of ^{116}Cd , the internal contamination of the $^{116}\text{CdWO}_4$ crystals by ^{110m}Ag , ^{228}Th and ^{234m}Pa , and the contribution from external γ quanta (“ γ ext.”). A peak of the $0\nu 2\beta$ decay of ^{116}Cd excluded at 90% C.L. is shown too (a). The difference between the experimental energy spectrum and the Monte Carlo background model (points with error bars) together with the excluded peak of the $0\nu 2\beta$ decay of ^{116}Cd (solid line) (b).

90% C.L. In accordance with [70], we took $\lim S = 19.1$ counts that can be excluded at 90% C.L. Taking into account the detection efficiency $\eta = 0.9597$ (the part of simulated events remaining in the whole energy distribution due to escape of β particles and bremsstrahlung γ quanta), the new limit on the $0\nu 2\beta$ decay of ^{116}Cd to the ground state of ^{116}Sn is set as:

$$T_{1/2} \geq 2.2 \times 10^{23} \text{ yr} \quad \text{at 90\% C.L.}$$

Similar estimations can be obtained for the experimental sensitivity, by using simple consideration of the background statistics in the region of interest. The total number of events in the energy interval (2720–2920) keV (where 81.43% of the peak is concentrated) is 113 counts that leads to a $\lim S = 20.3$ counts at 90% C.L. according to the procedure proposed by Feldman and Cousins for an expected background and no true signal (Table XII in [70]). The approach provides a half-life limit $T_{1/2} \geq 1.7 \times 10^{23}$ yr. Another estimation of $\lim S = 17.4$ counts can be obtained as $1.64 \times \sqrt{N_{\text{BG}}}$, where $N_{\text{BG}} = 113$ is number of background counts in the energy interval (2720–2920) keV. It corresponds to the half-life limit $T_{1/2} \geq 2.0 \times 10^{23}$ yr, that again is near to the result obtained from the fit.

Assuming the mass mechanism of $0\nu 2\beta$ decay with light neutrino exchange, we can estimate a limit on the effective Majorana neutrino mass $\langle m_\nu \rangle$ by using the following equation for the $0\nu 2\beta$ decay rate:

$$[T_{1/2}^{0\nu}]^{-1} = g_A^4 G^{0\nu} |M^{0\nu}|^2 \frac{\langle m_\nu \rangle^2}{m_e^2}, \quad (5)$$

where g_A is the axial vector coupling constant, $G^{0\nu}$ is the phase space factor that depends on Z and the nuclear transition energy $Q_{2\beta}$, $M^{0\nu}$ is the NME for $0\nu 2\beta$ decay, m_e is the electron mass. In our analysis, we use the phase space factor from [68] and the axial vector coupling constant $g_A = 1.27$. By using the recent $M^{0\nu}$ obtained in the framework of the density functional theory based on a nonrelativistic [26] and a relativistic [29] energy density functional theory, the quasiparticle random-phase approximation [25], the proton-neutron quasiparticle random-phase approximation [27], and the microscopic interacting boson model [19] we have obtained the following interval of the effective Majorana neutrino mass limits:

$$\langle m_\nu \rangle \leq (1.0 - 1.7) \text{ eV} \quad \text{at 90\% C.L.}$$

The obtained limits on half-life and on the effective Majorana neutrino mass are compared with the limits of other experiments in Fig. 14. Neutrinoless 2β decay can be mediated by different mechanisms, particularly by hypothetical right-handed currents admixture in the weak interaction. The following limits were set on the parameters of the admixtures using calculations [44,71,72]:

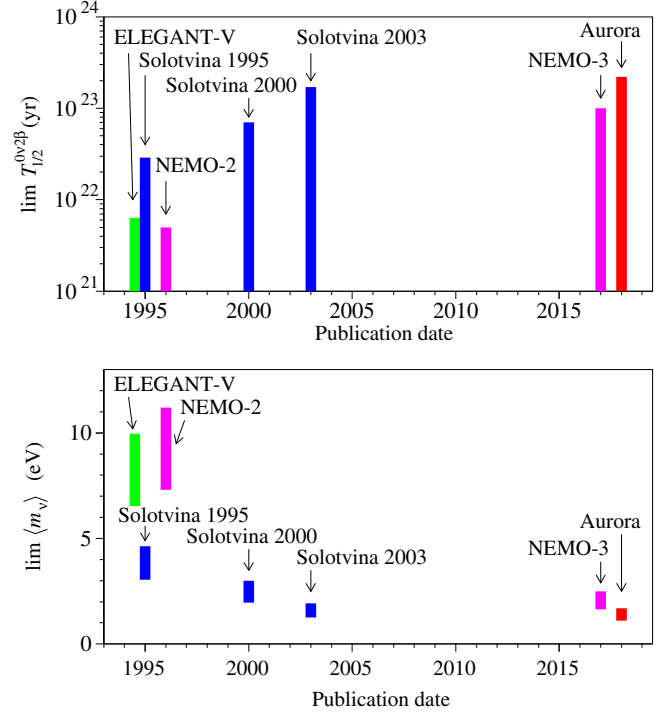


FIG. 14. Comparison of the ^{116}Cd $0\nu 2\beta$ half-life limits obtained in the Aurora experiment with other experiments: ELEGANT V [40], Solotvina (three stages of the experiment published in 1995, 2000 and 2003) [32,41,42], NEMO-2 [44], and NEMO-3 [45] (upper panel). Comparison of the effective Majorana neutrino mass limits obtained in the Aurora experiment with estimations of $\langle m_\nu \rangle$ limits obtained in the other experiments. The intervals of the effective Majorana neutrino mass limits were calculated by using the phase space factor from [68], the axial vector coupling constant $g_A = 1.27$, and the same $M^{0\nu}$ that have been utilized to estimate the neutrino-mass limits interval in the present experiment [19,25–27,29] (lower panel).

$\langle \eta \rangle \leq (1.6 - 21) \times 10^{-8}$ and $\langle \lambda \rangle \leq (1.8 - 22) \times 10^{-6}$. In accordance with [73], the value of the coupling constant λ'_{111} in the R-parity violating minimal supersymmetric standard model is restricted by the $T_{1/2}^{0\nu}$ limit to $\lambda'_{111} \leq 2.5 \times 10^{-4} \times f$ at 90% C.L., where $f = (m_{\tilde{q}}/100 \text{ GeV})^2 \times (m_{\tilde{g}}/100 \text{ GeV})^{1/2}$; $m_{\tilde{q}}$ and $m_{\tilde{g}}$ are the squark and gluino masses. Also an interval of lower limits on the heavy neutrino mass was estimated assuming the $0\nu 2\beta$ decay mechanism of exchanging by heavy Majorana neutrino. By using the nuclear matrix elements ($M^{0\nu_h} = 110 - 302$) calculated in [19,27,29,74], the phase-space factor ($G_{0\nu} = 16.7 \times 10^{-15} \text{ yr}^{-1}$) from [68], and $g_A = 1.27$ the mass of heavy Majorana neutrino is restricted as $|\langle m_{\nu_h}^{-1} \rangle|^{-1} \geq (10 - 28) \times 10^6 \text{ GeV}$.

C. Search for 2β transitions to excited levels of ^{116}Sn

The 2β decay can also proceed through transitions to excited levels of the daughter nucleus. Studies of the latter transitions allow to extract supplementary information about the 2β process. Up to now $2\nu 2\beta$ decay to the first

0^+ excited state of daughter nuclei was detected in ^{100}Mo and ^{150}Nd (see review [75]). The theoretical predictions for such transition in ^{116}Cd are on the level of $T_{1/2} \sim 10^{21} - 10^{24}$ yr (see review [75]). So, there is a chance to detect this transition in ^{116}Cd too. As it was noted in [76], the detection of $0\nu 2\beta$ transition to excited levels would give an additional possibility to distinguish mechanisms of the $0\nu 2\beta$ decay if observed.

We set limits on 2β transition to several lowest excited levels of ^{116}Sn by fit of the data in different energy intervals. For instance, the energy spectrum measured by the $^{116}\text{CdWO}_4$ detectors over 26831 h was fitted in the energy intervals from (700–1300) keV to (3200–4000) keV by the model similar to the one used for the $2\nu 2\beta$ decay of ^{116}Cd to the ground state of ^{116}Sn with added simulated distribution of $2\nu 2\beta$ decay of ^{116}Cd to the first excited $0^+ 1757$ keV level of ^{116}Sn . The best fit, achieved in the energy interval (700–3800) keV ($\chi^2/\text{n.d.f.} = 1.13$), provides area of the effect 2111 ± 1807 counts, that gives no evidence for the effect searched for. The $\text{lim } S = 5075$ counts (at 90% C.L.) can be obtained assuming Gaussian errors [70]. Taking into account the detection efficiency 88.94% we get a half-life limit $T_{1/2} \geq 5.9 \times 10^{20}$ yr. The excluded distribution of the $2\nu 2\beta$ decay of ^{116}Cd to the first excited $0^+ 1757$ keV level of ^{116}Sn is shown in Fig. 15(a).

For the $0\nu 2\beta$ decay of ^{116}Cd to the first excited $0^+ 1757$ keV level of ^{116}Sn , the highest sensitivity was achieved by analysis of the data recorded with the $^{116}\text{CdWO}_4$ detectors over 35324 h. The spectrum, see Fig. 15(b), was fitted in the energy intervals from (1500–2000) keV to (3200–4000) keV by the same model, however, without contribution from internal and external ^{40}K . In this case, the best fit was achieved in the energy interval 1980–3900 keV ($\chi^2/\text{n.d.f.} = 0.964$) with the effect area -7 ± 57 counts that again gives no evidence of the effect observation. An estimation of $\text{lim } S = 87$ counts (90% C.L.) was obtained by using the Feldman-Cousins recommendations [70]. The detection efficiency for the neutrinoless transition is 88.23%, that leads to the half-life limit $T_{1/2} \geq 4.5 \times 10^{22}$ yr. Limits on other 2β transitions of ^{116}Cd to excited levels of ^{116}Sn were obtained in a similar way. They are presented in Table VI, where results of the most sensitive previous experiments are given for comparison.

D. Search for 2β decay with majoron emission and Lorentz violation

Spontaneous violation of global $B - L$ symmetry in gauge theories leads to the existence of a massless Goldstone boson, the majoron (χ^0). The majoron, if it exists, could play a significant role in the history of the early Universe and in the evolution of stars. In addition, majoron could play the role of the dark matter particle

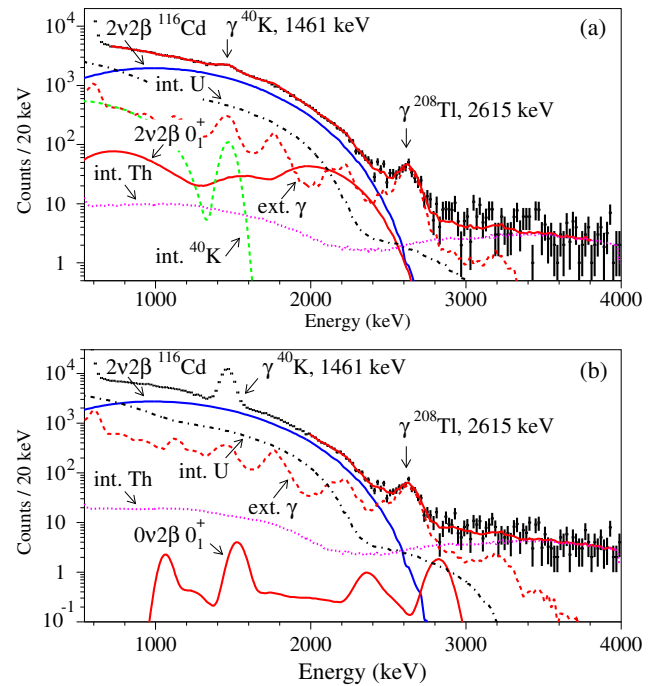


FIG. 15. The energy spectra of $\gamma(\beta)$ events measured by the $^{116}\text{CdWO}_4$ detectors over 26831 h (a) and 35324 h (b), corrected on the efficiency of the PSD and front-edge cuts, together with the main components of the background model: the g.s. to g.s. $2\nu 2\beta$ decay of ^{116}Cd , internal contaminations of the $^{116}\text{CdWO}_4$ crystals by U/Th, K (“int. U”, “int. Th”, “int. ^{40}K ”), and contributions from external γ quanta (“ext. γ ”). The fit and the excluded distributions of the $2\nu 2\beta$ (a) and $0\nu 2\beta$ (b) decay of ^{116}Cd to the first excited $0^+ 1757$ keV level of ^{116}Sn are shown too.

(see, for example, [78,79]). In the original majoron models, the majoron is part of an electroweak singlet [80,81], doublet [82], or triplet [83]. The models of a doublet and triplet majoron were disproved in 1989 by the data on the decay width of the Z^0 boson that were obtained at the LEP [84]. Despite this, some new models were proposed [85,86], where $0\nu \chi^0 2\beta$ decay is possible and where there are no contradictions with the LEP data. A 2β decay model that involves the emission of two majorons was proposed within Supersymmetric theories [87], and several other models of the majoron were proposed in the 1990s. By the term “majoron” one means massless or light bosons that are associated with neutrinos. In these models, the majoron can carry a lepton charge and is not required to be a Goldstone boson [88,89]. A decay process that involves the emission of two majorons is also possible [87,90]. In models featuring a vector majoron, the majoron is the longitudinal component of a massive gauge boson emitted in 2β decay [91]. In the work [92] a “bulk” majoron model was proposed in the context of the “brane-bulk” scenario for particle physics. Classification of majoron models (related to 2β decay) can be found in [77]. The shape of the two-electron energy sum distribution depends on the “spectral index” n defined by the phase space of the emitted particles

$G \sim (Q_{2\beta} - T)^n$, where $Q_{2\beta}$ is the energy released in the decay and T is the energy of the two electrons (the ordinary $2\nu 2\beta$ decay has the spectral index $n = 5$). The single majoron decay $2\beta\chi^0$ is possible with $n = 1, 2$ and 3 . The models for the emission of two majorons $2\beta\chi^0\chi^0$ correspond to $n = 3$ and 7 . The half-life for ordinary majoron with spectral index $n = 1$ can be written as:

$$[T_{1/2}^{0\nu\chi^0}]^{-1} = G_{0\nu\chi^0} \cdot g_A^4 \cdot \langle g_{ee} \rangle^2 \cdot |M_{0\nu\chi^0}|^2, \quad (6)$$

where $G_{0\nu\chi^0}$ is the phase space factor (which is accurately known [93]), $M_{0\nu\chi^0}$ is the nuclear matrix element (the same as for $0\nu\beta\beta$ decay), $\langle g_{ee} \rangle$ is the coupling constant of the majoron to the neutrino, and g_A is the axial-vector coupling constant.

In decay with emission of two majorons, we have

$$[T_{1/2}^{0\nu\chi^0\chi^0}]^{-1} = G_{0\nu\chi^0\chi^0} \cdot g_A^4 \cdot \langle g_{ee} \rangle^4 \cdot |M_{0\nu\chi^0\chi^0}|^2. \quad (7)$$

The Lorentz invariance (LI) is one of the founding principles of modern physics, but it could be only approximate symmetry of our local spacetime possibly modified at some scale outside of our experience. As any fundamental principle, LI should be checked with the highest available to-date sensitivity (see, for example, reviews [94,95]). As it was noted in [23,96], LI could be tested also in 2β decay experiments as LI violation leads to energy spectra of emitted particles different from those in usual $2\nu 2\beta$ process. This alteration of the electron-sum spectrum in the $2\nu 2\beta$ decay has been explored by the EXO-200 experiment, obtaining the first experimental limit on the relevant coefficient for the Lorentz violation (LV) [97]. In addition, *CPT*-violating Majorana couplings in the standard model extensions can trigger $0\nu 2\beta$ decay even for a negligible Majorana mass [96].

Search for the $0\nu 2\beta$ decay with majorons emission and $2\nu 2\beta$ Lorentz-violating decay was realized by using an approach similar to the utilized for the investigations of the 2β decay to the excited levels of ^{116}Sn . For instance, the experimental energy spectrum gathered over 35324 h was analyzed to set a limit on the $0\nu 2\beta$ decay with single majoron emission ($n = 1$). The fit in the energy interval (2200–3860) keV ($\chi^2/\text{n.d.f.} = 1.13$) gives an area of the simulated distribution 113 ± 241 counts that corresponds to $\text{lim } S = 533$ counts (the fit and excluded $0\nu\chi^0$ distribution are shown in Fig. 16, a). Taking into account the detection efficiency of the decay (98.38%) the half-life limit can be set as $T_{1/2}^{0\nu\chi^0} (n=1) \geq 8.2 \times 10^{21}$ yr at 90% C.L. Limits on other possible neutrinoless double-beta processes with majorons emission and the Lorentz-violating $2\nu 2\beta$ decay were set in a similar way (see Fig. 17). All the results of the experiment are summarized in Table VI.

Using the limit on the $0\nu 2\beta$ decay with majoron emission with $n = 1$, the phase space integral calculations [93], and

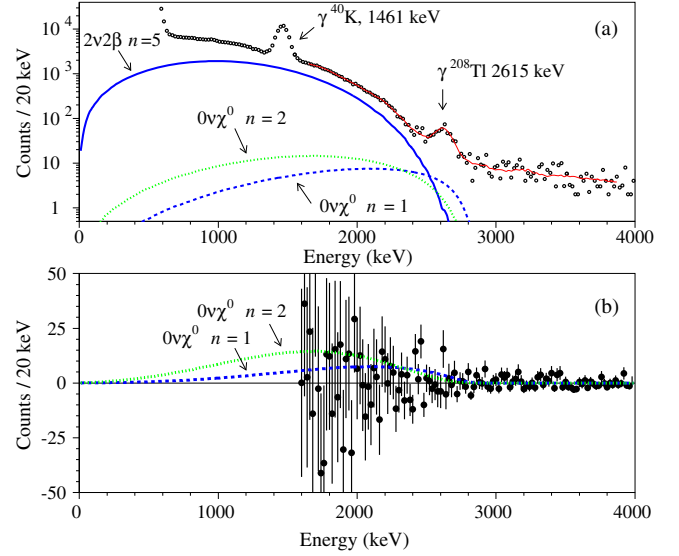


FIG. 16. Energy spectrum of $^{116}\text{CdWO}_4$ detectors acquired over 35324 h. The fit of the data, the $2\nu 2\beta$ spectrum of ^{116}Cd and excluded at 90% C.L. distributions for neutrinoless double-beta decay of ^{116}Cd with majorons emission ($n = 1$ and $n = 2$) are shown (a). Difference between the experimental data and the background model together with the excluded distributions (b).

the axial vector coupling constant $g_A = 1.27$, we get an upper limit on the coupling constant with the majoron emission $\langle g_{ee} \rangle \leq (6.1 - 9.3) \times 10^{-5}$.

To derive the limits on $\langle g_{ee} \rangle$ in other models with one or two majoron(s) emissions and $n = 3, 7$, we used the

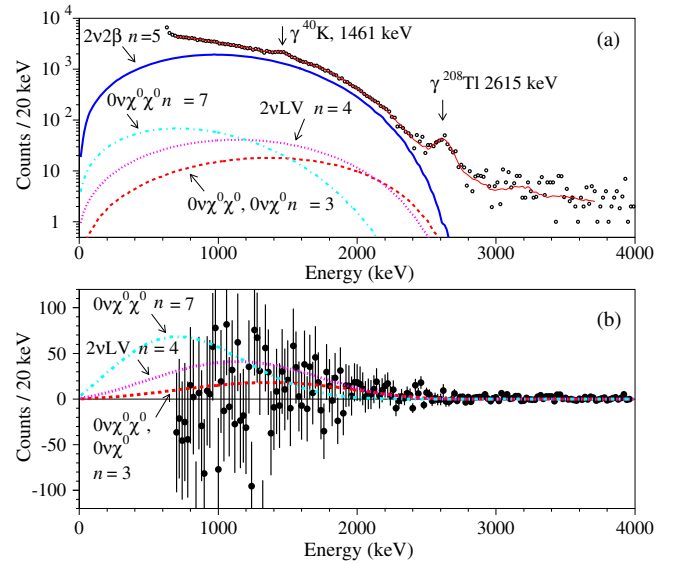


FIG. 17. Energy spectrum of $^{116}\text{CdWO}_4$ detectors acquired over 26831 h. The fit of the data, the $2\nu 2\beta$ spectrum of ^{116}Cd and excluded at 90% C.L. distributions for neutrinoless double-beta decay of ^{116}Cd with majorons emission ($n = 3$ and $n = 7$), and for Lorentz-violating ($n = 4$) $2\nu 2\beta$ decay of ^{116}Cd are shown (a). Difference between the experimental data and the background model together with the excluded distributions (b).

TABLE VI. Summary of the obtained results on 2β processes in ^{116}Cd . The limits are given at 90% C.L., except of the results of [47], obtained at 68% C.L.

Decay mode	Transition, level of ^{116}Sn (keV)	$T_{1/2}$ (yr)	Best previous limits (yr) Reference
2ν	g.s.	$(2.63^{+0.11}_{-0.12}) \times 10^{19}$ yr	see Table I and Fig. 12
2ν	2^+ (1294)	$\geq 9.8 \times 10^{20}$	$\geq 2.3 \times 10^{21}$ [48]
2ν	0^+ (1757)	$\geq 5.9 \times 10^{20}$	$\geq 2.0 \times 10^{21}$ [48]
2ν	0^+ (2027)	$\geq 1.1 \times 10^{21}$	$\geq 2.0 \times 10^{21}$ [48]
2ν	2^+ (2112)	$\geq 2.5 \times 10^{21}$	$\geq 1.7 \times 10^{20}$ [47]
2ν	2^+ (2225)	$\geq 7.5 \times 10^{21}$	$\geq 1.0 \times 10^{20}$ [47]
0ν	g.s.	$\geq 2.2 \times 10^{23}$	$\geq 1.7 \times 10^{23}$ [32]
0ν	2^+ (1294)	$\geq 7.1 \times 10^{22}$	$\geq 2.9 \times 10^{22}$ [32]
0ν	0^+ (1757)	$\geq 4.5 \times 10^{22}$	$\geq 1.4 \times 10^{22}$ [32]
0ν	0^+ (2027)	$\geq 3.1 \times 10^{22}$	$\geq 0.6 \times 10^{22}$ [32]
0ν	2^+ (2112)	$\geq 3.7 \times 10^{22}$	$\geq 1.7 \times 10^{20}$ [47]
0ν	2^+ (2225)	$\geq 3.4 \times 10^{22}$	$\geq 1.0 \times 10^{20}$ [47]
$0\nu\chi^0 n = 1$	g.s.	$\geq 8.2 \times 10^{21}$	$\geq 8.5 \times 10^{21}$ [45]
$0\nu\chi^0 n = 2$	g.s.	$\geq 4.1 \times 10^{21}$	$\geq 1.7 \times 10^{21}$ [32]
$0\nu\chi^0 n = 3$	g.s.	$\geq 2.6 \times 10^{21}$	$\geq 0.8 \times 10^{21}$ [32]
$0\nu\chi^0\chi^0 n = 3$	g.s.	$\geq 2.6 \times 10^{21}$	$\geq 0.8 \times 10^{21}$ [32]
$2\nu LV n = 4$	g.s.	$\geq 1.2 \times 10^{21}$...
$0\nu\chi^0\chi^0 n = 7$	g.s.	$\geq 8.9 \times 10^{20}$	$\geq 4.1 \times 10^{19}$ [77]

nuclear matrix elements and the phase space factors calculated in [98]. The results are given in Table VII.

In the Lorentz-violated $2\nu 2\beta$ decay [96], the differential decay rate is described by expression

$$d\Gamma/dt_1 dt_2 = C \cdot e_1 p_1 F(t_1, Z) \cdot e_2 p_2 F(t_2, Z) \cdot [(t_0 - t_1 - t_2)^5 + 10a_{\text{of}}^{(3)}(t_0 - t_1 - t_2)^4], \quad (8)$$

where C is the normalizing constant, t_i is the kinetic energy of the i th electron (all energies here are in units of the electron mass $m_e c^2$), $e_i = t_i + 1$ is the total energy of i th particle, p_i is its momentum $p_i = \sqrt{t_i(t_i + 2)}$ (in units of $m_e c$), t_0 is the energy release, and $F(t, Z)$ is the Fermi function which takes into account the influence of the electric field of the nucleus on the emitted electrons (Z is atomic number of the daughter nucleus). Thus, the shape and the total rate in the LV- $2\nu 2\beta$ decay are different in comparison to the usual $2\nu 2\beta$ process. The total rate is:

$$\Gamma = \Gamma_{2\nu} + \Gamma_{2\nu LV}, \quad (9)$$

where

$$\Gamma_{2\nu} = CI_5, \quad \Gamma_{2\nu LV} = 10a_{\text{of}}^{(3)} \cdot CI_4, \quad (10)$$

TABLE VII. Limits on lepton-number violating parameters. The limits are given at 90% C.L.

Parameter	Limit
Effective light Majorana neutrino mass $\langle m_\nu \rangle$	$\leq (1.0 - 1.7)$ eV
Effective heavy Majorana neutrino mass $ \langle m_{\nu_h}^{-1} \rangle ^{-1}$	$\geq (10 - 28) \times 10^6$ GeV
Right-handed current admixture $\langle \lambda \rangle$	$\leq (1.8 - 22) \times 10^{-6}$
Right-handed current admixture $\langle \eta \rangle$	$\leq (1.6 - 21) \times 10^{-8}$
Coupling constant of neutrino with majoron $\langle g_{ee} \rangle$	
$\chi^0, n = 1$	$\leq (6.1 - 9.3) \times 10^{-5}$
$\chi^0, n = 3$	$\leq 7.7 \times 10^{-2}$
$\chi^0\chi^0, n = 3$	$\leq (0.69 - 6.9)$
$\chi^0\chi^0, n = 7$	$\leq (0.57 - 5.7)$
R-parity violating parameter λ'_{111}	$\leq 2.5 \times 10^{-4} \times f$ (see text)
Lorentz-violating parameter $a_{\text{of}}^{(3)}$	$\leq 4.0 \times 10^{-6}$ GeV

$$I_5 = \int_0^{t_0} dt_1 e_1 p_1 F(t_1, Z) \times \int_0^{t_0-t_1} dt_2 e_2 p_2 F(t_2, Z) (t_0 - t_1 - t_2)^5, \quad (11)$$

$$I_4 = \int_0^{t_0} dt_1 e_1 p_1 F(t_1, Z) \times \int_0^{t_0-t_1} dt_2 e_2 p_2 F(t_2, Z) (t_0 - t_1 - t_2)^4. \quad (12)$$

The LV amplitude (or its limit) can be find as

$$10a_{\text{of}}^{(3)} = \frac{\Gamma_{2\nu LV}}{\Gamma_{2\nu}} \cdot \frac{I_5}{I_4} = \frac{T_{1/2}^{2\nu}}{T_{1/2}^{2\nu LV}} \cdot \frac{I_5}{I_4}. \quad (13)$$

The I_4, I_5 integrals can be calculated numerically using tabulated values of the Fermi function [99].³ With the values obtained in this work: $T_{1/2}^{2\nu} = 2.63 \times 10^{19}$ yr and $\lim T_{1/2}^{2\nu LV} = 1.2 \times 10^{21}$ yr, we get limit $a_{\text{of}}^{(3)} \leq 4.0 \times 10^{-6}$ GeV, at the same level as that obtained in the EXO-200 experiment for ^{136}Xe .

A summary on limits on lepton-number violating parameters obtained in the present work is given in Table VII.

³Using the Primakoff-Rosen approximation [100] $F(t, Z) \sim e/p$ (which works well for β^- and $2\beta^-$ decays), it is possible to calculate the integrals analytically: $I_5 = t_0^7(t_0^4 + 22t_0^3 + 220t_0^2 + 990t_0 + 1980)/83160$, $I_4 = t_0^6(t_0^4 + 20t_0^3 + 180t_0^2 + 360t_0 + 1260)/37800$. This gives: $a_{\text{of}}^{(3)} = (T_{1/2}^{2\nu}/T_{1/2}^{2\nu LV}) \times 4.55 \times 10^{-2} \times Q_{2\beta} \cdot (t_0^4 + 22t_0^3 + 220t_0^2 + 990t_0 + 1980)/(t_0^4 + 20t_0^3 + 180t_0^2 + 360t_0 + 1260)$.

V. CONCLUSIONS

The Aurora experiment to investigate 2β processes in ^{116}Cd with 1.162 kg of enriched $^{116}\text{CdWO}_4$ scintillators is finished after about five years of data taking at the Gran Sasso underground laboratory of I.N.F.N. (Italy). The half-life of ^{116}Cd relative to the $2\nu 2\beta$ decay to the ground state of ^{116}Sn is measured with the highest up-to-date accuracy: $T_{1/2} = (2.63_{-0.12}^{+0.11}) \times 10^{19}$ yr. The statistical error of the value is negligible (0.4%), while the main sources of the systematic error are the uncertainties of the background model and of the detector energy scale, and the pulse-shape discrimination cuts efficiency. Two-neutrino and neutrinoless 2β transitions of ^{116}Cd to several excited levels of ^{116}Sn are restricted at the level of $T_{1/2} > 10^{20} - 10^{22}$ yr.

A new half-life limit on the $0\nu 2\beta$ decay of ^{116}Cd to the ground state of ^{116}Sn is set as $T_{1/2} \geq 2.2 \times 10^{23}$ yr at 90% C.L., that corresponds to the effective Majorana neutrino mass limits $\langle m_\nu \rangle \leq (1.0-1.7)$ eV, depending on the nuclear matrix elements used in the analysis. Neutrinoless $0\nu 2\beta$ decay with different majorons emission

were investigated with sensitivity $T_{1/2} > 10^{21} - 10^{22}$ yr. New limits for the hypothetical right-handed currents admixtures in weak interaction, the heavy neutrino mass, and for the effective majoron-neutrino coupling constants were set on the basis of the obtained $T_{1/2}$ limits. Search for Lorentz-violating $2\nu 2\beta$ decay of ^{116}Cd was realized for the first time resulting in the most stringent limit on the Lorentz-violating parameter $a_{\text{of}}^{(3)} \leq 4.0 \times 10^{-6}$ GeV.

ACKNOWLEDGMENTS

The group from the Institute for Nuclear Research (Kyiv, Ukraine) was supported in part by the program of the National Academy of Sciences of Ukraine “Fundamental research on high-energy physics and nuclear physics (international cooperation).” F. A. D. gratefully acknowledges support from the Jean d’Alembert fellowship program (project CYGNUS) of the Paris-Saclay Excellence Initiative, Grant No. ANR-10-IDEX-0003-02. A. S. B., S. I. K., V. N. S., and V. I. U. were supported by the Russian Science Foundation (Grant No. 18-12-00003).

-
- [1] V. I. Tretyak and Yu. G. Zdesenko, *At. Data Nucl. Data Tables* **80**, 83 (2002).
 - [2] R. Saakyan, *Annu. Rev. Nucl. Part. Sci.* **63**, 503 (2013).
 - [3] A. S. Barabash, *Nucl. Phys.* **A935**, 52 (2015).
 - [4] J. D. Vergados, H. Ejiri, and F. Šimkovic, *Int. J. Mod. Phys. E* **25**, 1630007 (2016).
 - [5] H. Päs and W. Rodejohann, *New J. Phys.* **17**, 115010 (2015).
 - [6] S. M. Bilenky and C. Giunti, *Int. J. Mod. Phys. A* **30**, 1530001 (2015).
 - [7] S. Dell’Oro, S. Marcocci, M. Viel, and F. Vissani, *Adv. High Energy Phys.* **2016**, 2162659 (2016).
 - [8] A. Giuliani and A. Poves, *Adv. High Energy Phys.* **2012**, 857016 (2012).
 - [9] O. Cremonesi and M. Pavan, *Adv. High Energy Phys.* **2014**, 951432 (2014).
 - [10] X. Sarazin, *J. Phys. Conf. Ser.* **593**, 012006 (2015).
 - [11] R. Arnold *et al.* (NEMO-3 Collaboration), *Phys. Rev. D* **92**, 072011 (2015).
 - [12] A. Gando *et al.* (KamLAND-Zen Collaboration), *Phys. Rev. Lett.* **117**, 082503 (2016).
 - [13] J. B. Albert *et al.* (EXO-200 Collaboration), *Phys. Rev. Lett.* **120**, 072701 (2018).
 - [14] C. Alduino *et al.* (CUORE Collaboration), *Phys. Rev. Lett.* **120**, 132501 (2018).
 - [15] C. E. Aalseth *et al.* (A2 Collaboration), *Phys. Rev. Lett.* **120**, 132502 (2018).
 - [16] M. Agostini *et al.* (GERDA Collaboration), *Phys. Rev. Lett.* **120**, 132503 (2018).
 - [17] O. Azzolini *et al.*, *Phys. Rev. Lett.* **120**, 232502 (2018).
 - [18] J. Engel and J. Menendez, *Rep. Prog. Phys.* **80**, 046301 (2017).
 - [19] J. Barea, J. Kotila, and F. Iachello, *Phys. Rev. C* **91**, 034304 (2015).
 - [20] J. Kostensalo, M. Haaranen, and J. Suhonen, *Phys. Rev. C* **95**, 044313 (2017).
 - [21] J. Abad *et al.*, *J. Phys. Colloques* **45**, C3 (1984).
 - [22] A. S. Barabash, A. D. Dolgov, R. Dvornický, F. Šimkovic, and A. Yu. Smirnov, *Nucl. Phys.* **B783**, 90 (2007).
 - [23] J. S. Diaz, V. A. Kostelecky, and R. Lehnert, *Phys. Rev. D* **88**, 071902(R) (2013).
 - [24] M. Wang, G. Audi, F. G. Kondev, W. J. Huang, S. Naimi, and X. Xu, *Chin. Phys. C* **41**, 030003 (2017).
 - [25] F. Šimkovic, V. Rodin, A. Faessler, and P. Vogel, *Phys. Rev. C* **87**, 045501 (2013).
 - [26] N. L. Vaquero, T. R. Rodriguez, and E. J. Luis, *Phys. Rev. Lett.* **111**, 142501 (2013).
 - [27] J. Hyvärinen and J. Suhonen, *Phys. Rev. C* **91**, 024613 (2015).
 - [28] J. M. Yao, L. S. Song, K. Hagino, P. Ring, and J. Meng, *Phys. Rev. C* **91**, 024316 (2015).
 - [29] L. S. Song, J. M. Yao, P. Ring, and J. Meng, *Phys. Rev. C* **95**, 024305 (2017).
 - [30] J. Meija *et al.*, *Pure Appl. Chem.* **88**, 293 (2016).
 - [31] F. A. Danevich *et al.*, *Phys. Rev. C* **67**, 014310 (2003).
 - [32] F. A. Danevich *et al.*, *Phys. Rev. C* **68**, 035501 (2003).
 - [33] P. Belli *et al.*, *Phys. Rev. C* **76**, 064603 (2007).
 - [34] P. Belli *et al.*, *Eur. Phys. J. A* **36**, 167 (2008).
 - [35] P. Belli *et al.*, *Phys. Rev. C* **85**, 044610 (2012).
 - [36] P. Belli *et al.*, *Phys. Rev. C* **93**, 045502 (2016).

- [37] G. Wang *et al.*, [arXiv:1504.03599v1](#).
- [38] A. Giuliani, F. A. Danevich, and V. I. Tretyak, *Eur. Phys. J. C* **78**, 272 (2018).
- [39] J. Blachot, *Nucl. Data Sheets* **111**, 717 (2010).
- [40] H. Ejiri *et al.*, *J. Phys. Soc. Jpn.* **64**, 339 (1995).
- [41] F. A. Danevich, A. Sh. Georgadze, V. V. Kobychiev, B. N. Kropivyansky, V. N. Kuts, A. S. Nikolaiko, V. I. Tretyak, and Yu. Zdesenko, *Phys. Lett. B* **344**, 72 (1995).
- [42] F. A. Danevich *et al.*, *Phys. Rev. C* **62**, 045501 (2000).
- [43] R. Arnold *et al.*, *JETP Lett.* **61**, 170 (1995).
- [44] R. Arnold *et al.*, *Z. Phys. C* **72**, 239 (1996).
- [45] R. Arnold *et al.*, *Phys. Rev. D* **95**, 012007 (2017).
- [46] A. S. Barabash, *Phys. Rev. C* **81**, 035501 (2010).
- [47] A. S. Barabash, A. V. Kopylov, and V. I. Cherehovskiy, *Phys. Lett. B* **249**, 186 (1990).
- [48] A. Piepke *et al.*, *Nucl. Phys.* **A577**, 493 (1994).
- [49] A. S. Barabash *et al.*, Proc. 4th International Conference on Current Problems in Nuclear Physics and Atomic Energy (NPAE-Kyiv2012), Kyiv (National Academy of Sciences of Ukraine, Ukraine, 2013), p. 353.
- [50] D. V. Poda *et al.*, *EPJ Web Conf.* **65**, 01005 (2014).
- [51] O. G. Polischuk *et al.*, *AIP Conf. Proc.* **1686**, 020017 (2015).
- [52] F. A. Danevich *et al.*, *J. Phys. Conf. Ser.* **718**, 062009 (2016).
- [53] O. G. Polischuk *et al.*, *AIP Conf. Proc.* **1894**, 020018 (2017).
- [54] A. S. Barabash *et al.*, *J. Instrum.* **6**, P08011 (2011).
- [55] D. V. Poda *et al.*, *Radiation Measurements* **56**, 66 (2013).
- [56] F. A. Danevich *et al.*, *AIP Conf. Proc.* **1549**, 201 (2013).
- [57] E. Gatti and F. De Martini, *Proceedings of the Conference on Nuclear Electronics* Vol. II (International Atomic Energy Agency, Vienna, 1962), p. 265.
- [58] T. Fazzini, P. G. Bizzeti, P. R. Maurenzig, C. Stramaccioni, F. A. Danevich, V. V. Kobychiev, V. I. Tretyak, and Yu. G. Zdesenko, *Nucl. Instrum. Methods Phys. Res., Sect. A* **410**, 213 (1998).
- [59] L. Bardelli *et al.*, *Nucl. Instrum. Methods Phys. Res., Sect. A* **569**, 743 (2006).
- [60] A. S. Barabash *et al.*, *Nucl. Instrum. Methods Phys. Res., Sect. A* **833**, 77 (2016).
- [61] M. J. Koskelo, W. C. Burnett, and P. H. Cable, *Radioactivity and radiochemistry* **7**, 18 (1996).
- [62] V. I. Tretyak, *Astropart. Phys.* **33**, 40 (2010).
- [63] J. C. Barton and J. A. Edgington, *Nucl. Instrum. Methods Phys. Res., Sect. A* **443**, 277 (2000).
- [64] F. A. Danevich *et al.*, *Nucl. Phys.* **A694**, 375 (2001).
- [65] W. R. Nelson, H. Hirayama, and D. W. O. Rogers, The EGS4 code system report, Stanford Linear Accelerator Center SLAC Report No. SLAC-265, 1985.
- [66] O. A. Ponkratenko, V. I. Tretyak, and Yu. G. Zdesenko, *Phys. At. Nucl.* **63**, 1282 (2000); V. I. Tretyak (to be published).
- [67] M. Doi, T. Kotani, and E. Takasugi, *Prog. Theor. Phys. Suppl.* **83**, 1 (1985).
- [68] J. Kotila and F. Iachello, *Phys. Rev. C* **85**, 034316 (2012).
- [69] M. Mirea, T. Pahomi, and S. Stoica, *Romanian reports in Physics* **67**, 872 (2015).
- [70] G. J. Feldman and R. D. Cousins, *Phys. Rev. D* **57**, 3873 (1998).
- [71] A. Staudt, K. Muto, and H. V. Klapdor-Kleingrothaus, *Europhys. Lett.* **13**, 31 (1990).
- [72] G. Pantis, F. Šimkovic, J. D. Vergados, and A. Faessler, *Phys. Rev. C* **53**, 695 (1996).
- [73] A. Faessler, S. Kovalenko, and F. Šimkovic, *Phys. Rev. D* **58**, 115004 (1998).
- [74] A. Faessler, M. González, S. Kovalenko, and F. Šimkovic, *Phys. Rev. D* **90**, 096010 (2014).
- [75] A. S. Barabash, *AIP Conf. Proc.* **1894**, 020002 (2017).
- [76] F. Šimkovic and A. Faessler, *Prog. Part. Nucl. Phys.* **48**, 201 (2002).
- [77] R. Arnold *et al.*, *Nucl. Phys.* **A678**, 341 (2000).
- [78] M. Lattanzi, S. Riemer-Sørensen, M. Tórtola, and J. W. F. Valle, *Phys. Rev. D* **88**, 063528 (2013).
- [79] D. Kazanas, R. N. Mohapatra, S. Nasri, and V. L. Teplitz, *Phys. Rev. D* **70**, 033015 (2004).
- [80] Y. Chikashige, R. N. Mohapatra, and R. D. Peccei, *Phys. Rev. Lett.* **45**, 1926 (1980).
- [81] Y. Chikashige, R. N. Mohapatra, and R. D. Peccei, *Phys. Lett.* **98B**, 265 (1981).
- [82] C. Aulakh and R. N. Mohapatra, *Phys. Lett.* **119B**, 136 (1982).
- [83] G. Gelmini and M. Roncadelli, *Phys. Lett.* **99B**, 411 (1981).
- [84] C. Caso *et al.* (Particle Data Group), *Eur. Phys. J. C* **3**, 1 (1998).
- [85] R. N. Mohapatra and P. B. Pal, *Massive Neutrinos in Physics and Astrophysics* (World Scientific, Singapore, 1991).
- [86] Z. G. Berezhiani, A. Yu. Smirnov, and J. W. F. Valle, *Phys. Lett. B* **291**, 99 (1992).
- [87] R. N. Mohapatra and E. Takasugi, *Phys. Lett. B* **211**, 192 (1988).
- [88] C. P. Burgess and J. M. Cline, *Phys. Lett. B* **298**, 141 (1993).
- [89] C. P. Burgess and J. M. Cline, *Phys. Rev. D* **49**, 5925 (1994).
- [90] P. Bamert, C. P. Burgess, and R. N. Mohapatra, *Nucl. Phys.* **B449**, 25 (1995).
- [91] C. D. Carone, *Phys. Lett. B* **308**, 85 (1993).
- [92] R. N. Mohapatra, A. Perez-Lorenzana, and C. A. S. Pires, *Phys. Lett. B* **491**, 143 (2000).
- [93] J. Kotila, J. Barea, and F. Iachello, *Phys. Rev. C* **91**, 064310 (2015).
- [94] V. A. Kostelecky and N. Russel, *Rev. Mod. Phys.* **83**, 11 (2011).
- [95] J. D. Tasson, *Rep. Prog. Phys.* **77**, 062901 (2014).
- [96] J. S. Diaz, *Phys. Rev. D* **89**, 036002 (2014).
- [97] J. B. Albert *et al.* (EXO-200 Collaboration), *Phys. Rev. D* **93**, 072001 (2016).
- [98] M. Hirsch, H. V. Klapdor-Kleingrothaus, S. G. Kovalenko, and H. Päs, *Phys. Lett. B* **372**, 8 (1996).
- [99] H. Behrens and J. Janecke, *Numerical Tables for Beta-Decay and Electron Capture* (Springer-Verlag, Berlin, 1969).
- [100] H. Primakoff and S. P. Rosen, *Rep. Prog. Phys.* **22**, 121 (1959).